Check for updates

Geophysical Research Letters

RESEARCH LETTER
10.1029/2025GL121480

Magnetic Imaging of the Effect of Stress on the Remanent Magnetization of Basalt

A. R. Muxworthy[1,2,3], M. E. Kosters[3], B. M. de Groot[3], T. M. Mitchell[2], A. R. Thomson[2], B. Kugabalan[1], L. Qi[1], and L. V. de Groot[3]

[1]Department of Earth Science and Engineering, Imperial College London, London, UK, [2]Department of Earth Sciences, University College London, London, UK, [3]Palaeomagnetic Laboratory, Department of Earth Sciences, Utrecht University, Utrecht, The Netherlands

Key Points:

- Magnetic mapping confirms numerical predictions that magnetic moments can rotate under pressures <100 MPa
- Low stresses cause a net decrease in magnetic intensity, leading to underestimates of true paleointensity
- Low stresses near earthquakes or impacts can distort magnetic signals, so stress must be accounted for in paleomagnetic interpretation

Supporting Information:

Supporting Information may be found in the online version of this article.

Correspondence to:

A. R. Muxworthy,
adrian.muxworthy@imperial.ac.uk

Citation:

Muxworthy, A. R., Kosters, M. E., de Groot, B. M., Mitchell, T. M., Thomson, A. R., Kugabalan, B., et al. (2026). Magnetic imaging of the effect of stress on the remanent magnetization of basalt. *Geophysical Research Letters*, *53*, e2025GL121480. https://doi.org/10.1029/2025GL121480

Received 7 JAN 2026
Accepted 24 SEP 2026

Abstract Differential compressional stresses (<100 MPa) that do not result in permanent deformation have traditionally been considered insufficient to modify paleomagnetic signals; however, recent numerical predictions have challenged this assumption. Using quantum diamond microscopy, we experimentally determined the effects of low differential stresses on the remanent magnetization of columnar basalt samples from Seljadalur, Iceland. We show that although individual magnetic dipoles rotate by up to 40°, the bulk magnetization direction remains largely unchanged. These rotations reflect opposing single-domain–like and single-vortex–like behaviors that cancel directionally; however, the bulk magnetization intensity decreases. This behavior is consistent with micromagnetic model predictions for mixed–domain-state samples. Given that differential stresses ≪1 GPa are common in undeformed rocks distal to earthquake rupture zones and impact craters, it is essential to account for stress effects when interpreting paleomagnetic data from geological materials.

Plain Language Summary Magnetic particles in rocks store a long-term record of Earth's magnetic field, helping scientists reconstruct plate movements and field variations through time. Recent theoretical models have predicted that magnetic recordings in rocks can be affected by pressures much lower than previously thought, at levels too low to cause permanent damage to the rocks, for example, in regions distal to earthquake faults or impact craters. Here we use state-of-the-art Quantum Diamond Microscopy magnetic imaging to determine how individual magnetic dipoles carried by magnetic particles within a basalt from Iceland respond to compressive stresses. We demonstrate that many magnetic dipole orientations are strongly affected by stresses below 100 MPa, with reorientations of up to ~40°. As different sizes of magnetic particles can give rise to diametrically opposite responses, the net magnetization direction is often not altered; however, the net magnetization intensity is decreased. Low levels of stress, such as those found in rocks near but not directly affected by earthquakes or impacts, can therefore change how magnetic signals are recorded. This means that stress effects must be taken into account when interpreting paleomagnetic data.

1. Introduction

North et al. (2024) numerically predicted that differential stresses <100 MPa can strongly affect the paleomagnetic recording fidelity of magnetite within rocks and meteorites. These estimates are significantly lower than previous estimates that predicted that the paleomagnetic recordings of rocks were unaffected by stresses <1 GPa (Hodych, 1977; Nagata, 1971). These previous estimates were made using analytical theories for uniformly magnetized particles, so-called single-domain (SD) particles (Kittel, 1949). In contrast, the numerical predictions of North et al. (2024) were made using state-of-the-art numerical models that include non-uniform magnetizations, but more importantly these new predictions have been developed at a time when our understanding of how rocks retain geologically meaningful paleomagnetic recordings has been revolutionized (Nagy et al., 2022). We no longer assume that SD particles are the primary carrier of paleomagnetic signals, instead it is now known that the paleomagnetic signal of rocks is primarily carried by larger magnetic particles with non-uniform magnetizations, for example, >100 nm for magnetite (Gergov et al., 2025). These larger particles not only retain stable remanent magnetizations, but are often magnetically more stable than SD particles on geological timescales and carry larger magnetic moments (Gergov et al., 2025). Among these larger, non-uniformly magnetized grains, single-vortex (SV) particles, typically in the 100–1,000 nm size range for magnetite, are of particular interest

© 2026 The Author(s). Geophysical Research Letters published by Wiley Periodicals LLC on behalf of American Geophysical Union.
This is an open access article under the terms of the Creative Commons Attribution License, which permits use, distribution and reproduction in any medium, provided the original work is properly cited.

19448007, 2026, 19, Downloaded from https://agupubs.onlinelibrary.wiley.com/doi/10.1029/2025GL121480, Wiley Online Library on [07/11/2026]. See the Terms and Conditions (https://onlinelibrary.wiley.com/terms-and-conditions) on Wiley Online Library for rules of use; OA articles are governed by the applicable Creative Commons License

because of their high magnetic stability and widespread occurrence (Gergov et al., 2025). North et al. (2024) showed that it is the magnetizations of SV particles, which are easily affected by stresses <100 MPa.

Although these results initially appeared inconsistent with prevailing single-domain (SD) theory, laboratory experiments conducted over the past few decades (e.g., Hamano et al., 1989; Nagata, 1971; Schmidbauer & Petersen, 1968; Volk & Gilder, 2016) are broadly consistent with the predictions of North et al. (2024). These apparent discrepancies were commonly attributed to the presence of very large magnetic particles containing multiple magnetic regions, or domains, separated by domain walls, that is, so-called multidomain (MD) grains, typically ≫1,000 nm in magnetite. At the time, the existence of single-vortex (SV) particles was not recognized and was only identified later by Williams and Dunlop (1989). Because MD grains are generally thought not to retain significant magnetic remanence over geological timescales, stress-related effects observed in laboratory experiments were largely attributed to MD effects with less geological significance (Volk & Feinberg, 2019). However, this dismissal is not fully supported by the geological record, where there is evidence that paleomagnetic signals may have been permanently modified by relatively low stress levels (e.g., Salyards et al., 1992).

This reappraisal of laboratory and geological data, combined with the recent predictions of North et al. (2024), indicates that the paleomagnetic community may have underestimated the importance of stress on their data, with potentially far-reaching geological implications. For example, it may be necessary to introduce differential stress corrections to paleomagnetic data. These findings also opens up the possibility of new applications of paleomagnetic methods, such as using magnetic methods to estimate paleostresses around faults or impact structures. There is now a clear need for modern experimental studies to investigate the effects of stress on samples containing non-uniform magnetizations, in order to verify the findings of North et al. (2024). Kugabalan et al. (2026) have already begun to address this by studying the effect of stress on magnetic susceptibility; however, experiments on the magnetic recordings of rocks, that is, remanent magnetizations, are also urgently needed.

Here, we experimentally test the predictions of North et al. (2024) for remanent magnetizations recorded in rocks, by magnetically imaging the effect of uniaxial differential stress on basalts. To quantify the effect of stress, we use quantum diamond microscopy (QDM), which enables the study of magnetic behavior at the micron scale rather than at the bulk scale (Fu et al., 2020; Glenn et al., 2017).

2. Sample Description and Methods

A columnar basalt sample from Seljadalur, Iceland, sourced from the UCL rock collection, was selected for this study due to its relatively homogeneous composition (Browning et al., 2016; Vinciguerra et al., 2005). Previous studies have reported the sample's density as 2900 kg/m^3 ± 10 kg/m^3, with a porosity of ∼4% distributed uniformly throughout the rock (Browning et al., 2016). Kugabalan et al. (2026) also showed through optical and scanning electron microscopy (SEM), that the basalt is composed of inter-granular plagioclase, granular pyroxene, olivine and titanium-rich iron oxides. SEM grain-size analysis of the Ti-rich iron oxides with a resolution of ∼6 nm, found that the majority of the particles were between ∼50–3,000 nm, with a median of 534 nm (Kugabalan et al., 2026). For Ti-rich iron oxides this is predicted to be close to the SD/SV transition size, therefore, most of the particles in the basalt are expected to display SD or SV magnetic behavior (Cych et al., 2024).

To magnetically characterize the mineralogy of the basalt, high-temperature magnetic susceptibility curves (Muxworthy et al., 2023) were measured using an Agico MFK1-FA Kappabridge located at Imperial College London. To determine the magnetic domain state of the particles, which is related to grain-size, we measured first-order reversal curves (FORC) (Roberts et al., 2014) using a Princeton Measurements vibrating sample magnetometer (VSM) at Imperial. FORC data maps out the interior of major hysteresis loops, providing information about the coercive-force/particle-size distribution and the distribution of magnetostatic interactions (both internal and inter-particle) within a sample (Roberts et al., 2014).

The QDM measurements were made using an in-house-modified QDM.IO QDM at Utrecht University. The imaging was conducted post compression, that is, the samples were initially magnetically imaged using the QDM, compressed and then imaged again after the stress was released. To compress the samples, we used a Deben MICROTEST MT500 compression stage that is designed to be used in situ in an SEM. The size allowed for portability. For the compression experiments within the Deben compression stage, 6 mm diameter cores were cut, with a length of approximately 6 mm. To meet the standard requirement for compression experiments of a 2:1

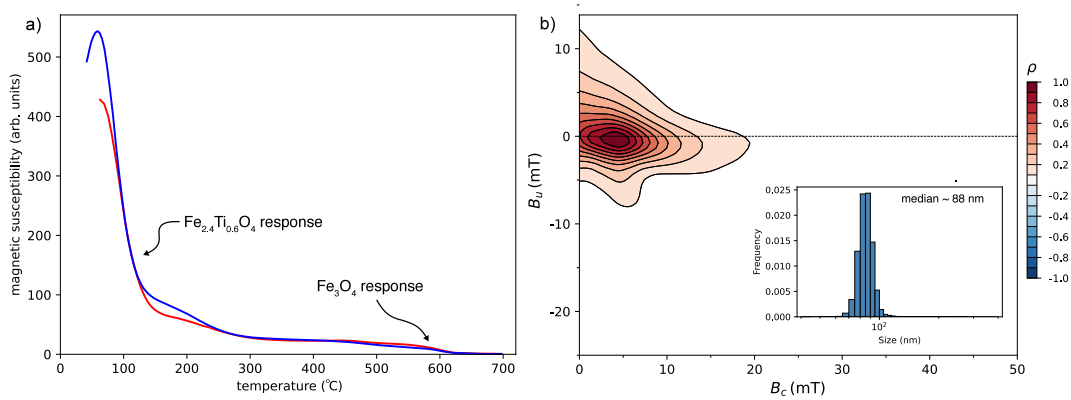


Figure 1. Rock magnetic characterization of the Seljadalur columnar basalt: (a) high-temperature susceptibility data, and (b) normalized FORC distribution. For the susceptibility measurements, heating was conducted in Ar. The FORC data was measured using 120 FORCs with an averaging time of 200 ms, and a smoothing factor of two (Roberts et al., 2014). A particle-size distribution estimate was made using FORCINN (Pei et al., 2025). As FORCINN assumes magnetite, we need to multiply the estimate by ∼5 to obtain an estimate for $Fe_{2.4}Ti_{0.6}O_4$.

ratio of length to width, a dummy core was used during compression to double the length. The samples were polished using a 0.5 μm diamond paste; during the compression experiment the polished surfaces were covered with Teflon tape for protection.

In addition to the magnetic measurements and QDM imaging, we obtained further SEM images to complement those used for the grain-size analysis of (Kugabalan et al., 2026), focusing on the specific areas examined during the QDM measurements. These images were acquired using a Hitachi TM4000 Plus SEM at Imperial.

3. Results

3.1. Magnetic Characterization Results

High-temperature susceptibility data revealed a main Curie temperature (strictly unblocking temperature) of ∼150°C, with a second much smaller peak at ∼590°C (Figure 1). The main Curie temperature corresponds to a titanomagnetite phase close to $Fe_{2.4}Ti_{0.6}O_4$ (Akimoto, 1962), which is often referred to as TM60 and is the main magnetic phase in most oceanic basalts (Petersen, 1984). The secondary higher-temperature peak indicates the presence of a near-magnetite-like phase. Ti-rich iron oxides are known to be more affected by stress than Ti-poor iron oxides (Sahu & Moskowitz, 1995).

The FORC distribution is indicative of a mixture of SD and SV behavior (Figure 1b), including particles near the low-stability transition zone (Nagy et al., 2017). Attempts to estimate the grain-size distribution using the FORCINN inversion algorithm (Pei et al., 2025) yielded a median grain size of ∼88 nm, significantly below the SEM-derived mean of 534 nm (Kugabalan et al., 2026). However, the FORCINN algorithm is based on the behavior of magnetite, which has a substantially lower SD to SV transition size (Cych et al., 2024). Based on the work of Cych et al. (2024), we need to multiply the FORCINN size estimate by ∼5 to obtain similar FORC behavior, that is, ∼440 nm, which is comparable to the published median of 534 nm (Kugabalan et al., 2026).

3.2. Magnetic Imaging

The samples were initially imaged using the QDM before compression, then compressed perpendicular to the imaging surface, that is, the z-axis, after which they were re-imaged. All QDM imaging was conducted under zero load.

One sample was initially magnetized with a saturation isothermal remanent magnetization (SIRM) at 45° to the measurement plane (Figure 2a) and then imaged. It was then compressed under a load of 59 MPa, with the peak load experienced for <10 s, the load released and the sample re-imaged using the QDM (Figure 2b).

For the initial processing of the QDM data we used QDMLab (Volk et al., 2022). For subsequent dipole fitting we used the iterative Euler deconvolution method of Souza-Junior et al. (2026); this iterative approach increases the

19448007, 2026, 19, Downloaded from https://agupubs.onlinelibrary.wiley.com/doi/10.1029/2025GL121480, Wiley Online Library on [07/11/2026]. See the Terms and Conditions (https://onlinelibrary.wiley.com/terms-and-conditions) on Wiley Online Library for rules of use; OA articles are governed by the applicable Creative Commons License

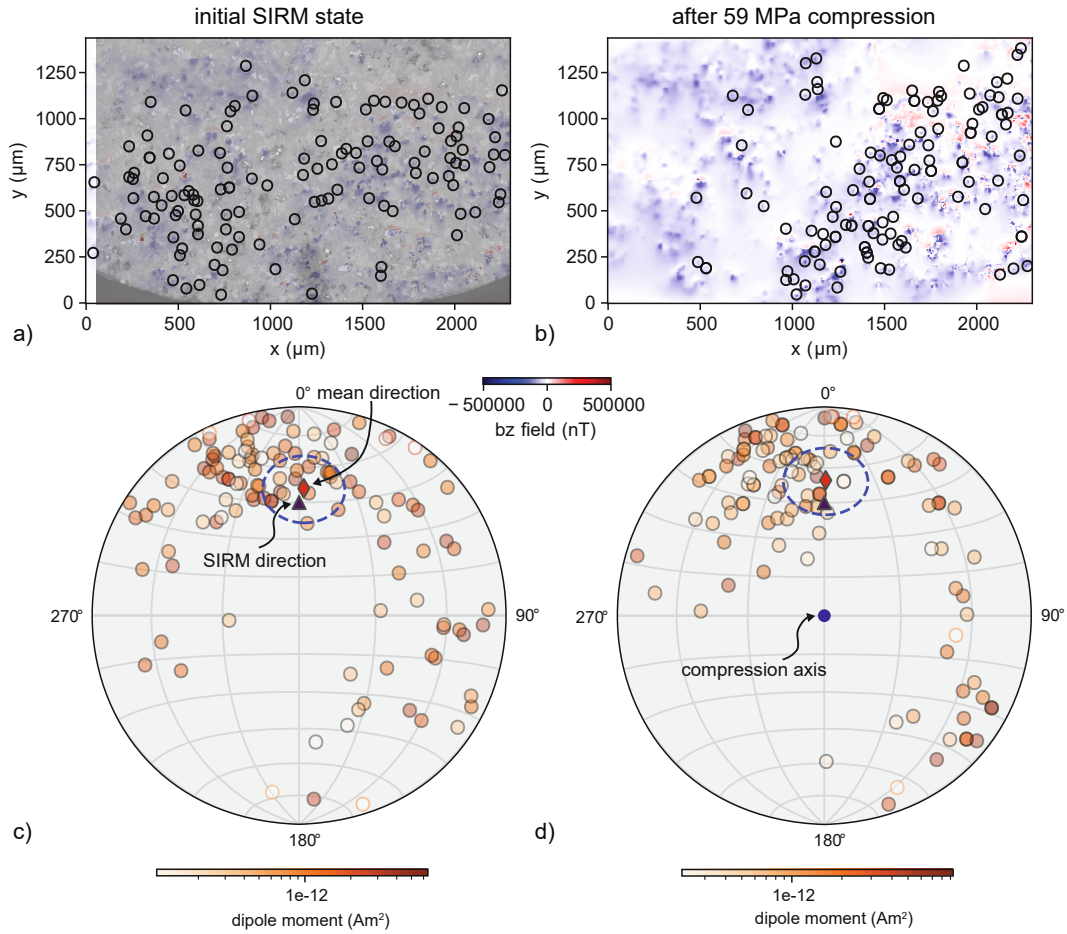


Figure 2. (a) QDM magnetic-field map of the initial SIRM state overlain on an SEM image of the same area (note the slight offset between the two images). Individual magnetic dipoles (circles) were identified using iterative Euler deconvolutional (Souza-Junior et al., 2026). (b) The same area of the sample after compression to 59 MPa with selected dipoles highlighted. (c) Equal-area projection plot of the direction of the dipoles highlighted in (a). (d) Equal-area projection plot of the directions of the dipoles highlighted in (b). In (c, d), the SIRM field direction and the mean dipole direction are shown, together with the corresponding α_{95} confidence ellipses. In (d) the compression axis is also highlighted.

number of dipole fits compared to the original approach detailed in Souza-Junior et al. (2024). We use this approach rather than a micromagnetic tomographic approach (de Groot et al., 2021) as the spatial distribution of the particles within the samples is unknown. Using a cut-off depth of 15 μm and a coefficient of determination for the dipole fit (R^2) >0.9 (Souza-Junior et al., 2024), we fitted 122 dipoles to the initial SIRM state (Figure 2a). For the post-59 MPa data, using the same criteria, we fitted 119 dipoles (Figure 2b). On plotting these dipole fits on equal-area projection plots and calculating the mean with α_{95} confidence limits, it is seen that both means plot within error of the SIRM direction which was imparted at 45° to the measurement plane (Figure 2); the mean of the initial SIRM state direction is slightly closer. The application of a compressive stress has been predicted (North et al., 2024) to rotate SD particles' magnetizations into the compression plane, and SV particle magnetizations toward the compression axis. Neither of these processes lead to a net rotation of the mean in this mixed-domain-state sample (Figure 1b), as the dipoles rotations cancel; however, at the individual dipole level rotations toward/away from the compression plane are expected. For example, there are less dipole fits aligned with the z-plane, for example, compare the 0°–180° dipole fits in Figures 2c and 2d, where it is seen that there are fewer dipole fits close to the z-plane. This will be analyzed further in the Discussion.

The NRM of another sister sample was imaged using the QDM (Figure 3). After imaging the NRM state, the sample was compressed in the z-plane, that is, the compression was perpendicular to the image plan. Increasing pressures were applied: 38, 67, 75, and 100 MPa; after each compression the load was released and the sample

19448007, 2026, 19, Downloaded from https://agupubs.onlinelibrary.wiley.com/doi/10.1029/2025GL121480, Wiley Online Library on [07/11/2026]. See the Terms and Conditions (https://onlinelibrary.wiley.com/terms-and-conditions) on Wiley Online Library for rules of use; OA articles are governed by the applicable Creative Commons License

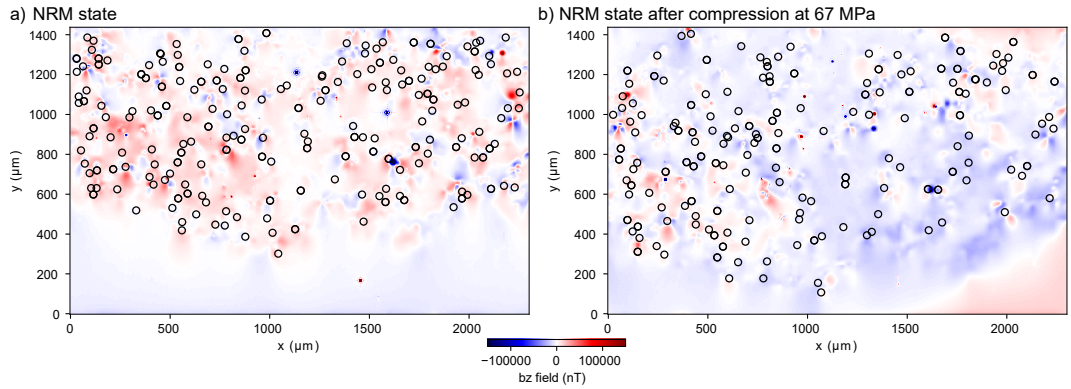


Figure 3. (a) QDM magnetic-field map of the initial NRM state in the second sample, with the dipoles selected by iterative Euler deconvolution (Souza-Junior et al., 2026) highlighted with circles. (b) The same area of the sample after compression to 67 MPa, with identified dipoles highlighted by circles.

imaged using the QDM. The data were processed using the same protocol as for the sample with the initial SIRM state (Figure 2), with two exceptions: a cut off depth of 30 μm was used and the R^2 cut-off reduced to >0.8. This yielded the corresponding number of dipole fits: 246, 278, 211, 243, and 241 using the procedure of Souza-Junior et al. (2026). The cut-off depth was increased, because in this particular sample there were not many dipoles/particles in the top 15 μm of the sample. The R^2 cut-off was also reduced to increase the number of identified dipoles. For the SIRM state (Figure 2), a higher R^2 cut-off (i.e., > 0.9) was required because much of the magnetic signal was effectively "washed out" by saturating the sample prior to measurement. As a result, individual dipoles were less well isolated, necessitating a higher R^2 threshold to reliably identify and characterize them. Previous studies, have a used a range of R^2 values, with values above 0.8 being shown to display reliable directional information (Bellon et al., 2026).

4. Discussion

The QDM analysis did not show significant net changes to the mean magnetization after compression in either the sample where a SIRM was imparted (Figure 2) or in the sample with the original NRM (Figure 3). This is not surprising, as the rock contains particles near to the SD to SV transition size for TM60 (Figure 1b). The numerical models of North et al. (2024) predict that SD and SV grains exhibit opposite responses to compressional stress, though SD behavior is more reversible on removal of stress. Consequently, samples containing mixtures of these two domain states may show little or no net bulk response owing to reversible behavior after the removal of stress and cancellation effects: SD magnetic moments tend to move into the compression plane - a randomization process—whereas SV magnetic moments align with the compression axis. The latter is likewise a randomization process, as the moment can align in either of two equivalent directions.

4.1. Individual Dipole Tracking and Analysis

To gain further insight into the response of particles to stress, we need to consider the response of individual dipoles. Whilst it is possible to determine the dipole field of an individual, isolated 50 nm particles using a QDM as has been shown by Kaub et al. (2026), it is important to realize that on a practical level the resolution of the QDM means that each dipole likely represents clusters of individual particles, which, if SD or SV, are of the order of ∼1,000 particles (Qi et al., 2025).

To study the behavior of individual dipoles, we needed to track their response to stress. We used an LED image-based registration approach (Evangelidis & Psarakis, 2008), to align and track particles between successive data sets; see Figure S1 in Supporting Information S1 for additional details. As part of the standard QDM measurement protocol, reflected-light LED images were acquired for each measurement state. These images were aligned to the initial data set, that is, the SIRM or NRM state, using an intensity-based image registration algorithm implemented in OpenCV/Python. The algorithm iteratively maximizes the correlation between pixel intensities to determine the optimal rigid in-plane transformation, consisting of both rotation and translation, required to align

19448007, 2026, 19, Downloaded from https://agupubs.onlinelibrary.wiley.com/doi/10.1029/2025GL121480, Wiley Online Library on [07/11/2026]. See the Terms and Conditions (https://onlinelibrary.wiley.com/terms-and-conditions) on Wiley Online Library for rules of use; OA articles are governed by the applicable Creative Commons License

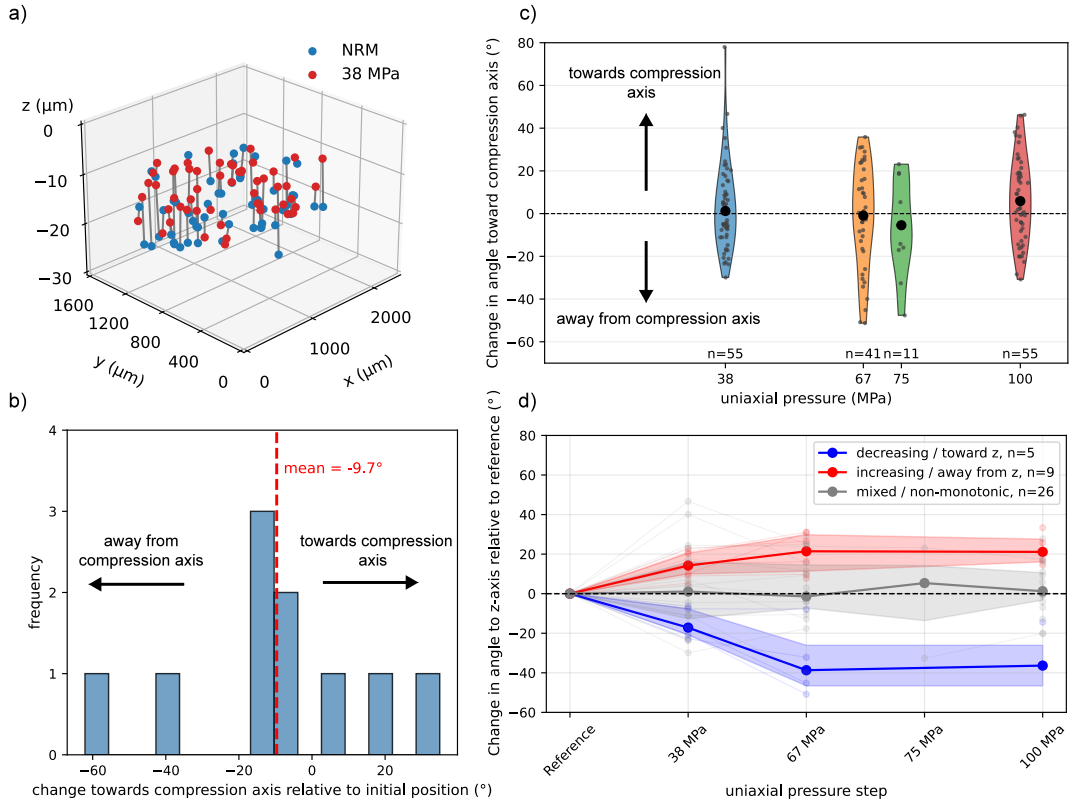


Figure 4. (a) An example of matching the dipole positions determined by iterative Euler deconvolution (Souza-Junior et al., 2026), for the NRM and post 38 MPa compression data sets following LED image-based registration and nearest-neighbor particle matching; note the contrasting scale between the *z* axis and the *x* and *y* axes. (b) Histogram showing the net rotation of identified dipoles toward or away from the compression axis after the initial SIRM state was compressed at 59 MPa (Figure 2). (c) Violin plot of the distribution of the rotation with respect to the initial NRM state for each of the four applied pressures (Figure 3). (d) Tracking of individual dipole rotation histories with increasing pressure, limited to dipoles identified after all four compressions. The behaviors fall into three categories: SV-like rotation toward the compression axis (decreasing angle to the compression axes), SD-like rotation away from it (increase) and dipoles showing no consistent trend. Mean behaviors are plotted with 95% confidence limits. In panels (b, c), rotation toward the compression axis is defined as positive, and away from it as negative.

each comparison image with the reference image. The resulting transformation was then applied to the corresponding dipole point clouds obtained from the iterative Euler deconvolution (Figures 2 and 3), including both the predicted source positions and magnetization directions. Following LED-image registration, individual dipoles were matched between the already aligned data sets using a mutual nearest-neighbor search within a positional tolerance of 30 μm. Additional nearest-neighbor separation criteria and bi-directional matching were applied to ensure robust one-to-one correspondences between dipoles. This allowed us to track the evolution of individual magnetic dipoles across multiple pressure steps.

It was clear from the images (e.g., Figure 3) that some dipoles would be common to all or several or the data sets, and some unique to individual data sets, that is, not all the dipoles were identified in every data set. In total this approach identified only 10 dipoles that were common to both of the SIRM data sets, that is, the initial state and the post-59 MPa compression state, and 40 dipoles that were common to at least four NRM data sets; the 75 MPa data set did not produce many dipole fits. The SIRM images were over saturated and not many dipole fits were successfully made compared to the NRM data.

The direction of the magnetization of each matched dipole after compression at 59 MPa was compared to the initial SIRM state, and the change in angle with respect to the compression axis determined (Figure 4b). The change in the net rotation toward or away from the compression axis is approximately zero, however, there are a number of dipoles that rotate toward the compression axis, and similarly many that rotate away, with rotations up

19448007, 2026, 19, Downloaded from https://agupubs.onlinelibrary.wiley.com/doi/10.1029/2025GL121480, Wiley Online Library on [07/11/2026]. See the Terms and Conditions (https://onlinelibrary.wiley.com/terms-and-conditions) on Wiley Online Library for rules of use; OA articles are governed by the applicable Creative Commons License

19448007, 2026, 19, Downloaded from https://agupubs.onlinelibrary.wiley.com/doi/10.1029/2025GL121480, Wiley Online Library on [07/11/2026]. See the Terms and Conditions (https://onlinelibrary.wiley.com/terms-and-conditions) on Wiley Online Library for rules of use; OA articles are governed by the applicable Creative Commons License

to 40°. These are the responses predicted by North et al. (2024) for SV-like and SD-like behaviors respectively. It is clear that significant rotations, that is >10°, can occur for particles at pressures as low at 59 MPa.

For the sample with the initial NRM state (Figure 3a), we have four increasing compressive stress data sets: 38, 67, 75, and 100 MPa. In Figure 4c, distributions of dipole rotations relative to the initial NRM state are plotted on a violin plot. The findings are similar to those for the SIRM in Figure 4b, that is, the mean deviation is close to zero, however, there is a wide distribution of dipole rotations, with many dipoles having rotated by >10° either toward or away from the compression axis. In Figure 4d, we identify the dipoles that are common to all five compressive stress data sets and plot their orientations as a function of angle relative to the compression axis. We group them into SV-like behavior (decreasing angle to the compression axes), SD-like behavior (increasing) or no clear trend. Given that each dipole represents the combined contribution of ∼1,000 or more particles, we would expect most dipoles to show no clear rotational trend given the magnetic particle-size distribution (Kugabalan et al., 2026). Although this indeterminate behavior is indeed the most common, it accounts for only about 65% of the observed particle responses. The remaining dipoles exhibit consistent increasing or decreasing trends, corresponding to regions likely dominated by either SD-like or SV-like behavior. Such textural heterogeneity has been reported previously in basalts (Gergov et al., 2025), indicating that magnetic particle sizes are not spatially uniform.

4.2. Comparison With Anisotropy of Magnetic Susceptibility Data

In a recent study, Kugabalan et al. (2026) reported the effect of stress on the anisotropy of magnetic susceptibility (AMS) in bulk sister samples from the same Seljadalur columnar blocks. They observed a pronounced stress dependence of the principal AMS axis, $\mathbf{K}_1$, which rotated toward the compression axis, with the degree of rotation increasing systematically with applied stress. Why is a comparable trend not observed in the mean dipole directions Figure 4? In our data, the mean dipole rotation remains close to zero.

The explanation is both contrasting and straightforward. In the dipole orientations derived from QDM imaging, individual dipoles can rotate either toward or away from a given vector direction. SD-like behavior corresponds to rotation away from that direction, whereas SV-like behavior corresponds to rotation toward it. For the Seljadalur sample, the distribution of SD- and SV-like responses is approximately equal (∼50:50), leading to an overall cancellation of the mean rotational signal. Additionally, some rotations toward the compression axis are 180° out of phase with the mean dipole moment, that is, dipoles can rotate either toward or away from the axis in two opposite senses.

In the AMS data, the behavior is more nuanced. Compression again causes both SV-like and SD-like moments to rotate, but susceptibility reflects the capacity of a moment to rotate from its current orientation. In other words, when a magnetic moment rotates under stress toward a given direction, its maximum susceptibility lies perpendicular to that new aligned direction; hence, $\mathbf{K}_1$ is perpendicular to the rotated magnetic moment's direction. This relationship means that both SD-like and SV-like AMS $\mathbf{K}_1$ axes are oriented perpendicular to their corresponding magnetic responses (Kugabalan et al., 2026; North et al., 2024). A second consideration is that AMS measures the response to preferred axes rather than preferred directions. Because the stresses applied in both this study and that of Kugabalan et al. (2026) are compressive, the stress is applied along an axis, that is, SV-like magnetic moments can rotate toward one of two directions. When we measure the AMS, this leads to an enhancement of the signal, however, when averaging the net moment of dipoles, this leads to a canceling effect.

4.3. Implications for Paleomagnetic Studies

Numerous laboratory studies have shown that differential stress can modify the magnetic state of rocks, with remanent magnetization varying under relatively modest pressures, typically below 1 GPa (e.g., Hamano et al., 1989; Nagata, 1971; Sato et al., 2021; Volk & Gilder, 2016). The long-recognized mismatch between theoretical predictions for ideal single-domain (SD) Stoner–Wohlfarth particles (Hodych, 1977; Nagata, 1971) and experimental observations is generally attributed to the influence of vortex (SV) or multidomain (MD) behavior (Volk & Feinberg, 2019). The micromagnetic models of North et al. (2024) provide a theoretical framework explaining why naturally occurring particles in rocks respond to stresses ≪1 GPa. Because magnetoelastic energy scales with the magnetostriction constant, TM60 has relatively high magnetostriction and should be more stress-sensitive than stoichiometric magnetite and many other common remanence carriers (Volk &

19448007, 2026, 19, Downloaded from https://agupubs.onlinelibrary.wiley.com/doi/10.1029/2025GL121480, Wiley Online Library on [07/11/2026]. See the Terms and Conditions (https://onlinelibrary.wiley.com/terms-and-conditions) on Wiley Online Library for rules of use; OA articles are governed by the applicable Creative Commons License

Feinberg, 2019). Its ubiquity in mid-ocean-ridge basalt also makes it directly relevant to oceanic crustal magnetization.

Such low differential stresses occur near faults, during mountain building and impacts (Lambert & Lapusta, 2023; North et al., 2023). For example, Kugabalan et al. (2026) suggested that AMS may provide a means to reconstruct paleostress orientations. For paleomagnetic directional and paleointensity data, the situation is more complex. Our QDM data show that individual dipoles can rotate significantly, while opposing rotations largely cancel in the net remanence direction but remain expressed in AMS.Such cancellation is expected in rocks containing mixtures of SD-like and SV-like particles, as in our Seljadalur sample. Directional changes should therefore be limited to a few degrees unless the grain-size distribution favors a single dominant state, potentially producing larger deflections.

Whilst the net paleomagnetic direction of samples containing SD-like and SV-like particles will be relatively unaltered due to canceling effects, there will be a net decrease in intensity (North et al., 2024). On conducting a standard modified-Thellier-type paleointensity experiment (e.g., Muxworthy et al., 2014), this net decrease in intensity will lead to both an underestimate of the true paleointensity and to non-linear behavior in the Arai diagram. This will occur because magnetic moments become thermally activated at temperatures unrelated to their original domain-state blocking, having been rotated and re-blocked under ambient stress conditions.

This conclusion is supported by previous experimental studies, for example, Volk and Gilder (2016) found that non-hydrostatic pressures reduced the paleointensity estimates by ∼20%. The implication for meteoritic samples is also potentially significant, as meteorites may have experienced multiple impacts in their history (e.g., Gattacceca et al., 2007; Steele et al., 2023), where the pressures are too low, that is, <5 GPa, to be accurately recorded petrographically (Scott et al., 1992). However, this will need to be quantified, as the effect of heating plays a significant role during high-velocity (high-strain-rate) events (North et al., 2023).

5. Conclusions

Through quantum diamond microscopy we have demonstrated that modest compressional differential stresses (<100 MPa) can produce significant rotations in individual magnetic dipoles, even though the bulk magnetization remains effectively unchanged (Figures 3 and 4). These dipole rotations are often >10°, and reflect contrasting SD-like and SV-like behaviors that cancel in the net mean paleomagnetic direction. The observations are consistent with micromagnetic models (North et al., 2024) that predict mixed domain states will exhibit opposing stress responses. Whilst the net paleomagnetic direction is not expected to be rotate significantly, the net magnetization intensity is expected to decrease leading to underestimates of the true paleointensity as has been previously reported (Volk & Gilder, 2016). On comparison with the work of Kugabalan et al. (2026), it is clear that AMS data is significantly more sensitive to stress than direction remanence data. This difference arises because differential stress and AMS measurements describe axial processes, whereas magnetic moments are vectorial, which leads to cancellation of stress effects rather than enhancement.

Collectively, the results show that low differential stresses ≪1 GPa, comparable to those in distal to earthquakes or impacts, can modify paleomagnetic signals, in particular magnetic intensity and AMS data. This underscores the need to consider stress effects when interpreting both AMS and paleomagnetic records in geological materials.

Conflict of Interest

The authors declare no conflicts of interest relevant to this study.

Availability Statement

All data used in this study are available from Muxworthy et al. (2025) and are openly accessible via Zenodo (http://doi.org/10.5281/zenodo.18018254).

Acknowledgments
A.R.M. acknowledges funding from UKRI EPSRC (EP/X02878X/1). B.K. acknowledges her Janet Watson PhD studentship.

References

Akimoto, S. (1962). Magnetic properties of FeO-Fe2O3-TiO2 system as a basis of rock magnetism. *Journal of the Physical Society of Japan*, *17*, 706. https://doi.org/10.1143/JPSJ.17.706

Bellon, U. D., Souza-Junior, G. F., Williams, A. R., Muxworthy, W., Uieda, L., Fu, R. R., & Trindade, R. I. F. (2026). Microscale pseudo-thellier palaeointensity using a quantum diamond microscope. *Research Square*. https://doi.org/10.21203/rs.3.rs-8864846/v1

Browning, J., Meredith, P., & Gudmundsson, A. (2016). Cooling-dominated cracking in thermally stressed volcanic rocks. *Geophysical Research Letters*, *43*(16), 8417–8425. https://doi.org/10.1002/2016GL070532

Cych, B., Paterson, G. A., Nagy, L., Williams, W., & Moskowitz, B. (2024). Magnetic domain states and critical sizes in the titanomagnetite series. *Journal of Geophysical Research: Solid Earth*, *129*(6), e2024JB028805. https://doi.org/10.1029/2024JB028805

de Groot, L. V., Fabian, K., Beguin, A., Kosters, M. E., Cortes-Ortuno, D., Fu, R. R., et al. (2021). Micromagnetic tomography for paleomagnetism and rock-magnetism. *Journal of Geophysical Research-Solid Earth*, *126*(10), e2021JB022364. https://doi.org/10.1029/2021jb022364

Evangelidis, G. D., & Psarakis, E. Z. (2008). Parametric image alignment using enhanced correlation coefficient maximization. *IEEE Transactions on Pattern Analysis and Machine Intelligence*, *30*(10), 1858–1865. https://doi.org/10.1109/TPAMI.2008.113

Fu, R. R., Lima, E. A., Volk, M. W. R., & Trubko, R. (2020). High-sensitivity moment magnetometry with the quantum diamond microscope. *Geochemistry, Geophysics, Geosystems*, *21*(8), e2020GC009147. https://doi.org/10.1029/2020gc009147

Gattacceca, J., Lamali, A., Rochette, P., Boustie, M., & Berthe, L. (2007). The effects of explosive-driven shocks on the natural remanent magnetization and the magnetic properties of rocks. *Physics of the Earth and Planetary Interiors*, *162*(1–2), 85–98. https://doi.org/10.1016/j.pepi.2007.03.006

Gergov, H., Muxworthy, A. R., Williams, W., & Cowan, A. C. (2025). Magnetic recording fidelity of basalts through 3d nanotomography. *Geochemistry, Geophysics, Geosystems*, *26*(3), e2024GC011776. https://doi.org/10.1029/2024GC011776

Glenn, D. R., Fu, R. R., Kehayias, P., Le Sage, D., Lima, E. A., Weiss, B. P., & Walsworth, R. L. (2017). Micrometer-scale magnetic imaging of geological samples using a quantum diamond microscope. *Geochemistry, Geophysics, Geosystems*, *18*(8), 3254–3267. https://doi.org/10.1002/2017gc006946

Hamano, Y., Boyd, R., Fuller, M., & Lanham, M. (1989). Induced susceptibility anisotropy of igneous rocks caused by uniaxial compression. *Journal of Geomagnetism and Geoelectricity*, *41*(2), 203–220. https://doi.org/10.5636/jgg.41.203

Hodych, J. P. (1977). Single-domain theory for reversible effect of small uniaxial stress upon the remanent magnetization rock. *Canadian Journal of Earth Sciences*, *14*, 2047–2061. https://doi.org/10.1139/e76-120

Kaub, L., Gilder, S. A., Fu, R. R., Maher, B. A., Maxemin, G., Kuan, A. T., et al. (2026). Magnetic dipole imaging of magnetite nanoparticles in brain tissue. *RSC Advances*, *16*(2), 983–994. https://doi.org/10.1039/D5RA08546B

Kittel, C. (1949). Physical theory of ferromagnetic domains. *Reviews of Modern Physics*, *21*(4), 541–583. https://doi.org/10.1103/RevModPhys.21.541

Kugabalan, B., Mitchell, T. M., Muxworthy, A. R., Williams, W., Gergov, H., Aben, F. M., et al. (2026). The magnetic signature of stress in rocks. *Geophysical Research Letters*, *53*(3), e2025GL119973. https://doi.org/10.1029/2025GL119973

Lambert, V., & Lapusta, N. (2023). Absolute stress levels in models of low-heat faults: Links to geophysical observables and differences for crack-like ruptures and self-healing pulses. *Earth and Planetary Science Letters*, *618*, 118277. https://doi.org/10.1016/j.epsl.2023.118277

Muxworthy, A. R., Kosters, M. E., de Groot, B. M., Mitchell, T. M., Thomson, A. R., Kugabalan, B., et al. (2025). Imaging the effect of stress on basalt samples [Dataset]. *Zenodo*. https://doi.org/10.5281/zenodo.18018254

Muxworthy, A. R., Krása, D., Williams, W., & Almeida, T. P. (2014). Paleomagnetic recording fidelity of nonideal magnetic systems. *Geochemistry, Geophysics, Geosystems*, *15*(6), 2254–2261. https://doi.org/10.1002/2014gc005249

Muxworthy, A. R., Turney, J. N., Qi, L., Baker, E. B., Perkins, J. R., & Abdulkarim, M. A. (2023). Interpreting high-temperature magnetic susceptibility data of natural systems. *Frontiers in Earth Science*, *11*, 1171200. https://doi.org/10.3389/feart.2023.1171200

Nagata, T. (1971). Introductory notes on shock remanent magnetization and shock demagnetization of igneous rocks. *Pure and Applied Geophysics*, *89*(1), 159–177. https://doi.org/10.1007/BF00875213

Nagy, L., Williams, W., Muxworthy, A. R., Fabian, K., Almeida, T. P., Ó Conbhuí, P., & Shcherbakov, V. P. (2017). Stability of equidimensional pseudo-single-domain magnetite over billion-year timescales. *Proceedings of the National Academy of Sciences of the United States of America*, *114*(39), 10356–10360. https://doi.org/10.1073/pnas.1708344114

Nagy, L., Williams, W., Tauxe, L., & Muxworthy, A. (2022). Chasing tails: Insights from micromagnetic modeling for thermomagnetic recording in non-uniform magnetic structures. *Geophysical Research Letters*, *49*(23), e2022GL101032. https://doi.org/10.1029/2022GL101032

North, T. L., Collins, G. S., Davison, T. M., Muxworthy, A. R., Steele, S. C., & Fu, R. R. (2023). The heterogeneous response of Martian meteorite Allan Hills 84001 to planar shock. *Icarus*, *390*, 115322. https://doi.org/10.1016/j.icarus.2022.115322

North, T. L., Muxworthy, A., Williams, W., Collins, G., Mitchell, T. M., & Davison, T. M. (2024). The effect of stress on palaeomagentic signals. *Geophysical Research Letters*, *51*, e2023GL106868. https://doi.org/10.1029/2023GL106868

Pei, Z., Williams, W., Nagy, L., Paterson, G. A., Moreno Ortega, R., Muxworthy, A. R., & Chang, L. (2025). FORCINN: First-order reversal curve inversion of magnetite using neural networks. *Geophysical Research Letters*, *52*(3), e2024GL112769. https://doi.org/10.1029/2024GL112769

Petersen, N. (1984). Ore mineralogy of south Atlantic basalts (deep sea drilling project leg 73). In K. Hsü, J. LaBrecque, & K. Pisciotto (Eds.), *Initial reports of the deep sea drilling project* (Vol. 73, pp. 603–606). U.S. Government Printing Office. https://doi.org/10.2973/dsdp.proc.73.122.1984

Qi, L., Muxworthy, A. R., Baker, E. B., Cao, X., Allerton, S., Bryson, J. F. J., & Zhang, Y. (2025). Quantifying serpentinization-driven remagnetization from ridge axis to subduction zone using quantum diamond microscopy. *Journal of Geophysical Research: Solid Earth*, *130*(10), e2025JB031606. https://doi.org/10.1029/2025JB031606

Roberts, A. P., Heslop, D., Zhao, X., & Pike, C. R. (2014). Understanding fine magnetic particle systems through use of first-order reversal curve diagrams. *Reviews of Geophysics*, *52*(4), 557–602. https://doi.org/10.1002/2014RG000462

Sahu, S., & Moskowitz, B. M. (1995). Thermal dependence of magnetocrystalline anisotropy and magnetostriction constants of single crystal $Fe_{2.4}Ti_{0.61}O_4$. *Geophysical Research Letters*, *22*(4), 449–452. https://doi.org/10.1029/94gl03296

Salyards, S. L., Sieh, K. E., & Kirschvink, J. L. (1992). Paleomagnetic measurement of nonbrittle coseismic deformation across the san andreas fault at pallett creek. *Journal of Geophysical Research*, *97*(B9), 12457–12470. https://doi.org/10.1029/92JB00194

Sato, M., Kurosawa, K., Kato, S., Ushioda, M., & Hasegawa, S. (2021). Shock remanent magnetization intensity and stability distributions of single-domain titanomagnetite-bearing basalt sample under the pressure range of 0.1–10 gpa. *Geophysical Research Letters*, *48*(8), e2021GL092716. https://doi.org/10.1029/2021GL092716

Schmidbauer, E., & Petersen, N. (1968). Some magnetic properties of two basalts under uniaxial compression measured at different temperatures. *Journal of Geomagnetism and Geoelectricity*, *20*(3), 169–180. https://doi.org/10.5636/jgg.20.169

Scott, E. R., Keil, K., & Stöffler, D. (1992). Shock metamorphism of carbonaceous chondrites. *Geochimica et Cosmochimica Acta*, *56*(12), 4281–4293. https://doi.org/10.1016/0016-7037(92)90268-N

Souza-Junior, G. F., Ueida, L., Trindade, R. I. F., Carmo, J., & Fu, R. (2024). Full vector inversion of magnetic microscopy images using euler deconvolution as prior information. *Geochemistry, Geophysics, Geosystems*, *25*(1), e2023GC011082. https://doi.org/10.1029/2023GC011082

19448007, 2026, 19, Downloaded from https://agupubs.onlinelibrary.wiley.com/doi/10.1029/2025GL121480, Wiley Online Library on [07/11/2026]. See the Terms and Conditions (https://onlinelibrary.wiley.com/terms-and-conditions) on Wiley Online Library for rules of use; OA articles are governed by the applicable Creative Commons License

Souza-Junior, G. F., Uieda, L., Trindade, R. I. F., Fu, R. R., Bellon, U. D., & Castro, Y. M. (2026). Robust directional analysis of magnetic microscopy images using non-linear inversion and iterative euler deconvolution. *Journal of Geophysical Research: Solid Earth*, *131*(4), e2025JB031725. https://doi.org/10.1029/2025JB031725

Steele, S. C., Fu, R. R., Volk, M. W., North, T. L., Brenner, A. R., Muxworthy, A. R., et al. (2023). Paleomagnetic evidence for a long-lived, potentially reversing Martian dynamo at 3.9 Ga. *Science Advances*, *9*(21), eade9071. https://doi.org/10.1126/sciadv.ade9071

Vinciguerra, S., Trovato, C., Meredith, P. G., & Benson, P. M. (2005). Relating seismic velocities, thermal cracking and permeability in mt. Etna and Iceland basalts. *Rock Physics and Geomechanics*, *42*(7), 900–910. https://doi.org/10.1016/j.ijrmms.2005.05.022

Volk, M. W. R., & Feinberg, J. M. (2019). Domain state and temperature dependence of pressure remanent magnetization in synthetic magnetite: Implications for crustal remagnetization. *Geochemistry, Geophysics, Geosystems*, *20*(5), 2473–2483. https://doi.org/10.1029/2019gc008238

Volk, M. W. R., Fu, R. R., Trubko, R., Kehayias, P., Glenn, D. R., & Lima, E. A. (2022). QDMlab: A MATLAB toolbox for analyzing quantum diamond microscope (QDM) magnetic field maps. *Computers Geosciences*, *167*, 105198. https://doi.org/10.1016/j.cageo.2022.105198

Volk, M. W. R., & Gilder, S. A. (2016). Effect of static pressure on absolute paleointensity recording with implications for meteorites. *Journal of Geophysical Research-Solid Earth*, *121*(8), 5596–5610. https://doi.org/10.1002/2016jb013059

Williams, W., & Dunlop, D. J. (1989). Three-dimensional micromagnetic modelling of ferromagnetic domain structure. *Nature*, *377*(6208), 634–637. https://doi.org/10.1038/337634a0

19448007, 2026, 19, Downloaded from https://agupubs.onlinelibrary.wiley.com/doi/10.1029/2025GL121480, Wiley Online Library on [07/11/2026]. See the Terms and Conditions (https://onlinelibrary.wiley.com/terms-and-conditions) on Wiley Online Library for rules of use; OA articles are governed by the applicable Creative Commons License